RSC Advances

ROYAL SOCIETY OF CHEMISTRY

www.rsc.org/advances

POSS-tethered fluorinated diblock copolymers with linear- and star-shaped topologies: Synthesis, self-assembled film and hydrophobic application

Aizhao Pan, Shao Yang, Ling He*

Department of Chemistry, School of Science, Xi'an Jiaotong University, Xi'an, China

Corresponding Author: Professor Ling He

Department of Chemistry, School of Science, Xi'an Jiaotong University

Xianning West Road, 28, Xi'an, 710049, China

Tel. +86-29-8266-8554; Fax: +86-29-8266-8559

E-mail: heling@mail.xjtu.edu.cn

Keywords

POSS;

Fluorinated block copolymer;

Linear and star-shaped;

Self-assembled micelle;

Film surface;

Hydrophobic application.

Abstract

Polyhedral oligomeric silsesquioxane (POSS) tethered fluorinated diblock copolymers with linear-shaped ap-POSS-PMMA-b-PDFHM and star-shaped *s*-POSS-(PMMA-b-PDFHM)$_{16}$ are synthesized by octakis(dibromoethyl) POSS (POSS-(Br)$_{16}$) and aminopropylisobutyl POSS (ap-POSS) initiating methylmethacrylate (MMA) and dodecafluoroheptylmethacrylate (DFHM). In THF solution, both diblock copolymers could self-assemble into 200 nm core/shell micelles as POSS/PDFHM core and 70-80 nm PMMA shell. These micelles are able to produce typical films as fluorine-rich topsurface and POSS-gathered subsurface. Although PDFHM segments and POSS cages are competitively migrating onto the film surface, the migration of PDFHM segments is actually improved by POSS cages. Comparatively, the surface of ap-POSS-PMMA-b-PDFHM film is much more rough and fluorine-rich than *s*-POSS-(PMMA-b-PDFHM)$_{16}$ film, therefore, ap-POSS-PMMA-b-PDFHM film gains higher viscoelasticity and higher oleophobicity, but a little lower hydrophobicity than-POSS-(PMMA-b-PDFHM)$_{16}$ film. The hydrophobic application of both linear- and star-shaped topologies are used to glass, cotton fabric and stone substrates reveals that the treated samples exhibit superhydrophobicity for cotton fabric (>150°) and obvious hydrophobicity for stone and glass (>135°) in resistance to water and other liquids like coffee, milk, coke and green tea. It is believed that the properties of self-assembled films and the hydrophobic application are related closely to the topologies of block copolymers.

1. Introduction

Self-assembled films have gained much attention in tailoring surface properties by migrating different segments in block copolymers onto the film surface.[1,2] For this reason, fluorinated block copolymers have been intensively studied for obtaining hydrophobic/oleophobic films due to their typical self-migration and self-orientation on the film surface.[3-6] Actually, manipulating the orientation of fluorinated block copolymer on the film surface is controlled by the block structure and the self-assembly behaviour of blocks in solvents.[7,8] Therefore, the development of advanced fluorinated block copolymers with extraordinary surface properties has been focused on an elaborate design of molecular structures and an absolute control over the self-assembly features in selective solvents.[3,5,8] Furthermore, the introducing of inorganic constituent into fluorinated block copolymers for self-assembled films is much promising in improving the surface properties of films.[3,5,9]

Polyhedral oligomeric silsesquioxanes (POSS) with cube-like structures as inorganic silica core surrounded by organic groups (such as alkyl, aryl, or any of their derivatives) [9,10] is normally used to produce well-defined POSS-containing polymers for improving the surface properties of films in obvious hydrophobicity, low surface energy, high thermostability and excellent surface properties.[11-20] Normally, the synthesis of POSS-containing polymers is focused on mono- and multi-functional POSS monomers.[21-23] Compared with mono-functional monomers for obtaining linear single-arm POSS-containing polymer,[24,25] the multi-functional POSS is possible to obtain hyperbranched or star-shaped polymers, such as eight-arm star-shaped polymer (POSS/PMMA-b-PS) grown from multi-initiator POSS-$(Cl)_8$ initiating methylmethacrylate (MMA) and styrene (St) by atom transfer radical polymerization (ATRP).[26]

When taking into account the excellent film surface by combining both POSS and fluoropolymer, the great potential with the wide applications has been developed,[27-31] such as a new POSS-end capped perfluorocyclobutyl (PFCB) aryl ether polymer with excellent process ability and higher degree of stability in nitrogen and air,[32] a transparent and superhydrophobic coating by combining fluorinated POSS and poly(vinylidene fluoride-co-hexafluoro propylene) (PVDF-HFP).[33] However, in order to fabricate self-assemble film by fluoropolymer-tethered POSS, the effect of POSS cages and fluoropolymer segments onto the self-assembled film is important to be understood, because our previous studies have confirmed that both POSS-contining copolymer and fluorinated copolymer could migrate onto the film surface during the film formation.[7,8,34]

In this paper, two topologies of POSS-tethered fluorinated diblock copolymers are synthesized by using octakis(dibromoethyl) POSS (POSS-$(Br)_{16}$) or aminopropylisobutyl POSS (for obtaining ap-POSS-Br) to initiate methylmethacrylate (MMA) and dodecafluoroheptylmethacrylate (DFHM) via ATRP approach, as shown in Scheme 1 for star-shaped *s*-POSS-(PMMA-b-PDFHM)$_{16}$ and with linear-shaped ap-POSS-PMMA-b-PDFHM. Their chemical structure and molecular weight are characterized by nuclear magnetic resonance (^{1}H-NMR and ^{13}C-NMR) and size exclusion chromatography (SEC). Their self-assembled micelles in tetrahydrofuran (THF) solution are observed by transmission electron microscopy (TEM), elemental mapping and energy dispersive X-ray spectrometer EDX. The casted film from these micelles is characterized for the surface roughness, surface chemical composition, surface water adsorption and viscoelasticity by atomic force microscope (AFM), X-Ray photoelectron spectroscopy (XPS), scanning electron microscopy coupled with an energy dispersive X-ray spectrometer (SEM-EDX) and Q-Sense E1 quartz crystal

microbalance with dissipation monitoring (QCM-D). Their hydrophobic application on glass, cotton fabric and stone substrate are compared by SEM and the water contact angles. We believe that this research contributes much to the relationship between the topologies and properties of POSS-tethered fluorinated diblock copolymers.

2. Experimental section

2.1 Materials

Octakis(dibromoethyl) polyhedral oligomeric silsesquioxane (POSS-$(Br)_{16}$, $C_{16}H_{24}Si_8O_{12}Br_{16}$, Mw=1911g·mol^{-1}, >99%wt) and aminopropylisobutyl POSS (ap-POSS, $C_{31}H_{71}NSi_8O_{12}$, Mw=874.58 g·mol^{-1}, >99%wt) were purchased from Hybrid Plastics Co. (USA) and were used as received. The white powder of ap-POSS-PMMA (Mn=16030 g·mol^{-1}, PDI=1.07) is prepared by ap-POSS and BiBB to obtain macroinitiator ap-POSS-Br and then to initiate MMA as the previous method.[34] Dodecafluoroheptyl methacrylate (DFHM, $C_{11}H_8O_2F_{12}$, liquid, Xuegia Fluorine-Silicon Chemical Company, China) and methyl methacrylate (MMA, $C_5H_8O_2$, 99%wt, Aldrich) were rinsed with 5%wt NaOH aqueous solution and then ion-free water until the rinsed water reaches pH=7, followed by drying over CaH_2 for 24 h and distilling under reduced pressure to remove inhibitor before use. N,N,N',N',N''-pentamethyldiethylenetriamine (PMDETA, 99%) was supplied by Aldrich and was used without further purification. Cyclohexanone and tetrahydrofuran (THF) were stirred over CaH_2 for 24 h at room temperature, and distilled under reduced pressure prior to use. Cuprous chloride (CuCl) was purified according to the previous method.[35] Methylene iodide (CH_2I_2, 98%) was supplied by Aladdin and was used without further purification.

2.2 Preparation of star-shaped diblock copolymer s-POSS-(PMMA-b-PDFHM)$_{16}$ by ATRP

After 0.4185g CuCl (4.185mmol) was added into a dry Schlenk tube which is sealed with a rubber septum prior to three vacuum/N_2 cycles, the mixture of POSS-$(Br)_{16}$ (0.5g, 0.2616mmol), MMA (8.3704g, 83.70mmol), PMDETA (0.9710g, 4.185mmol) and cyclohexanone (15g) were introduced into the tube under N_2 atmosphere. Reaction started at 80□ and last for 24 h in an oil bath with dry magnetic stirrer. The left catalyst was removed by passing the synthesis solution through an alumina column using THF as the solvent, and the excess solvent was removed under reduced pressure. When the colorless solution was reprecipitated into methanol and dried in a vacuum oven overnight, POSS-$(PMMA)_{16}$ was obtained as Scheme 1 in a yield of 82%. Afterwards, when 5g powder of POSS-$(PMMA)_{16}$ (0.1471mmol) was dissolved in 10g cyclohexanone in a Schlenk tube, 1.882g DFHM (0.4705mmol), 0.2354g CuCl (2.3536mmol) and 0.4071g PMDETA (2.3536mmol) were charged under N_2 atmosphere. Then, the reaction was permitted to last for 24 h at 110℃ in an oil bath as Scheme 1. The left catalyst and the excess solvent were removed by the same way as above. *s*-POSS-$(PMMA\text{-}b\text{-}PDFHM)_{16}$ was obtained in a yield of 58 %. The procedure, conditions and detailed recipes of polymerization were listed in Table 1.

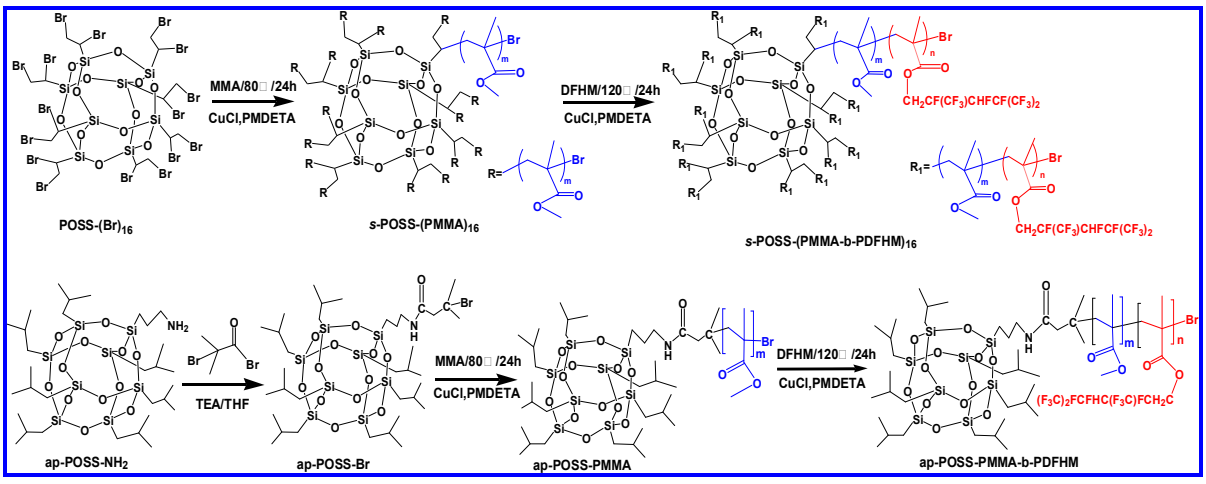

Scheme 1 Synthesis of *s*-POSS-$(PMMA\text{-}b\text{-}PDFHM)_{16}$ and ap-POSS-PMMA-b-PDFHM

2.3 Preparation of linear-shaped diblock copolymer ap-POSS-PMMA-b-PDFHM by ATRP

When 4.410g (0.2751mmol) ap-POSS-PMMA white powder (Mn=16030 g·mol^{-1}, PDI=1.07) was dissolved in 10g cyclohexanone in a Schlenk tube, 3.2g DFHM (8mmol), 0.02751g CuCl (0.2751mmol) and 0.04759g PMDETA (0.2751mmol) were introduced by constanous charging N_2, ap-POSS-PMMA-b-PDFHM was prepared by the same approach as *s*-POSS-(PMMA-b-PDFHM)$_{16}$ in Scheme 1 according the similar procedure as *s*-POSS-(PMMA-b-PDFHM)$_{16}$.

In order to compare, non-POSS initiator EiBB was used to synthesize diblock copolymer E-PMMA-b-PDFHM (Mn=34130 g·mol^{-1}, PDI=1.115) by ATRP as the same procedure (Table 1).

Table 1 The polymerization condition and detail recipes for prepared samples

Copolymer	Initiator/g	MMA/g	DFHM/g	CuCl/PMDETA/g	Cyclohexanone/g
POSS-(PMMA)$_{16}$	0.5 (POSS-(Br)$_{16}$)	8.3704	-	0.4185/0.9710	15
POSS-(PMMA-b-PDFHM)$_{16}$	5 (POSS-(PMMA)$_{16}$)	-	1.882	0.2354/0.4078	10
ap-POSS-PMMA	0.5426 (ap-POSS-Br)	5.30	-	0.06585/0.114	10
ap-POSS-PMMA-b-PDFHM	4.410 (ap-POSS-PMMA)	-	3.2	0.02751/0.04759	10
E-PMMA-b-PDFHM	5 (E-PMMA)	-	1.067	0.02973/0.05067	10

2.4 Characterization

Chemical structure. The nuclear magnetic resonance (^{1}H-NMR and ^{13}C-NMR) measurement for *s*-POSS-(PMMA-b-PDFHM)$_{16}$ and ap-POSS-PMMA-b-PDFHM was performed on a Bruker AV-500 spectrometer using $CDCl_3$ as solvent. Their molecular weight was determined on a DAWN EOS size exclusion chromatography (SEC) coupled with multiangle laser light scattering instrument (Wyatt Technology, USA) using SEC/DAWN EOS/Optilab rEX/QELS model. 0.01 mol·L^{-1} LiCl in THF solutiong was used as the eluent at a flow rate of 0.5 mL·min^{-1}.

Self-assembled micelles. The self-assembled micelles were prepared by 0.01 g·mL^{-1} solution of

s-POSS-(PMMA-b-PDFHM)$_{16}$ and ap-POSS-PMMA-b-PDFHM in THF. After filtering the solution through 0.45 μm disposable polyamide (PA) membrane, and keeping them for 30 minutes at room temperature, the morphology of self-assembled micelles was observed by transmission electron microscopy (TEM, JEM-3010) in an acceleration voltage of 100 kV. The micelle solutions were drop-casted onto carbon-coated copper grids, and then air-drying at room temperature before measurement. Elemental mapping and energy dispersive X-ray spectrometer EDX was performed on the X-ray spectrometers attached to the JEM-3010 instruments.

Casted films. The casted films were prepared by casting the micelle solutions (in THF, 2%wt) of *s*-POSS-(PMMA-b-PDFHM)$_{16}$ and ap-POSS-PMMA-b-PDFHM onto a glass and then drying it at ambient temperature. The topographies and roughness (root-mean-square roughness) of the films were characterized by atomic force microscope (AFM) unging NT-MDT new Solver-Next at room temperature under 38-42% R.H. Tip information: radius <10 nm, cantilever length 90±5 μm; width 40 ±3 μm; thickness 2.0±0.5 μm, resonant frequency 330 kHz, force constant 48 N/m. X-Ray photoelectron spectroscopy (XPS) measurement for elemental composition of surfaces was processed on the copolymer of the air-exposed film surface by an AXIS ULTRA (England, KRATOS ANALYTICAL Ltd) using an Al mono Kα X-ray source (1486.6 eV) operated at 150 W. The overview scans were obtained with pass energy of 160 eV and acquisition times of 220 s. Scanning electron microscopy coupled with an energy dispersive X-ray spectrometer (SEM-EDX, Hitachi Model 8010) was used to observe the cross section structure of film, the corresponding distribution of element at 1.0 kV accelerating potential. Q-Sense E1 quartz crystal microbalance with dissipation monitoring (QCM-D, Sweden) was used to measure the surface water adsorption and

viscoelasticity of film at 25℃. The Δf and ΔD were recorded at 15 MHz with air as the baseline.

Hydrophobic application. 10×10 cm cotton fabric (112g/m^2) and 2.5×2.5×1cm^3 stone samples (ρ=2.29g/cm^3) were immersed in the solution of linear- and star-shaped diblock copolymers (20 g/L) for 5 min. After padded through two dips and two nips to reach a wet pickup of 60-80%, the samples were dried at 80℃ for 5 min and heated at 120℃ for 5 min. The surface morphology was investigated by SEM. The surface contact angles measurements for 5μl deionized water and other liquids on the air-exposed treated surface on the treated glass, cotton fabric and stone were conducted on a OCA-20 DataPhysics Instruments GmbH with SCA 20 software at 25℃ (the average of at least five measurements).

3. Results and discussion

3.1 Chemical structure of linear- and star-shaped copolymers

In order to confirm the chemical structure of POSS-(PMMA-b-PDFHM)$_{16}$ and ap-POSS-PMMA-b-PDFHM, both ^{1}H-NMR and ^{13}C-NMR are conducted in Fig. 1. For POSS-(PMMA-b-PDFHM)$_{16}$, the typical δ_H (ppm, Fig.1a) at 5.5 (f, -O-C<u>H</u>$_2$- in PDFHM), 4.5 (e, -C<u>H</u>F- in PDFHM), 3.62 (a, -OC<u>H</u>$_3$ in PMMA), 1.86 (b, -CH$_2$-C<u>H</u>(CH$_3$)$_2$ in POSS), 1.03-0.95 (d, -C<u>H</u>$_3$ in POSS) and 0.85 (c, R-C<u>H</u>$_3$ in PMMA and PDFHM) have confirmed its diblock structure as designed in Scheme 1, after compared with the typical δ_H of POSS-(Br)$_{16}$ (ppm) at 3.65 (b, Si-C<u>H</u>(CH$_2$)Br), 3.8/4.05 (a^2/a^1, CH-C<u>H</u>$_2$-Br), and the typical δ_H of POSS-(PMMA)$_{16}$ (ppm) at 3.60 (a, -OCH$_3$ in PMMA), 1.86 (b, Si-C<u>H</u>(CH$_2$)-R in POSS), 1.56 (d, -C<u>H</u>$_2$- in PMMA) and 0.85 (c, R-CH$_3$ in PMMA) in Fig. S1. Furthermore, ^{13}C-NMR in Fig. 1b also proves the diblock structure of POSS-(PMMA-b-PDFHM)$_{16}$ by the typical δ_C (ppm) at 178.5 (-<u>C</u>O-O- in PMMA and PDFHM) and

120-125 ($\underline{C}F(\underline{C}F_3)\underline{C}HF\underline{C}F(\underline{C}F_3)_2$ in PDFHM). For ap-POSS-PMMA-b-PDFHM in Fig. 1a, ^{1}H-NMR (δ_H, ppm) at 0.60 (-Si-C$\underline{H}_2$- in POSS), 0.80 (c, R-C$\underline{H}_3$ in PMMA and PDFHM), 1.05-0.98 (d, -C$\underline{H}_3$ in POSS), 1.86 (b, -CH$_2$-C$\underline{H}$(CH$_3$)$_2$ in POSS), 3.60 (a, -OC$\underline{H}_3$ in PMMA), 5.5 (f, -O-C$\underline{H}_2$- in PDFHM) and 4.5 (e, -C$\underline{H}$F- in PDFHM), together with ^{13}C-NMR (ppm) at 178.5 (-$\underline{C}$O-O- in PMMA and PDFHM) and 120-125 ($\underline{C}F(\underline{C}F_3)\underline{C}HF\underline{C}F(\underline{C}F_3)_2$ in PDFHM), indicate its diblock structure as designed in Scheme 1.

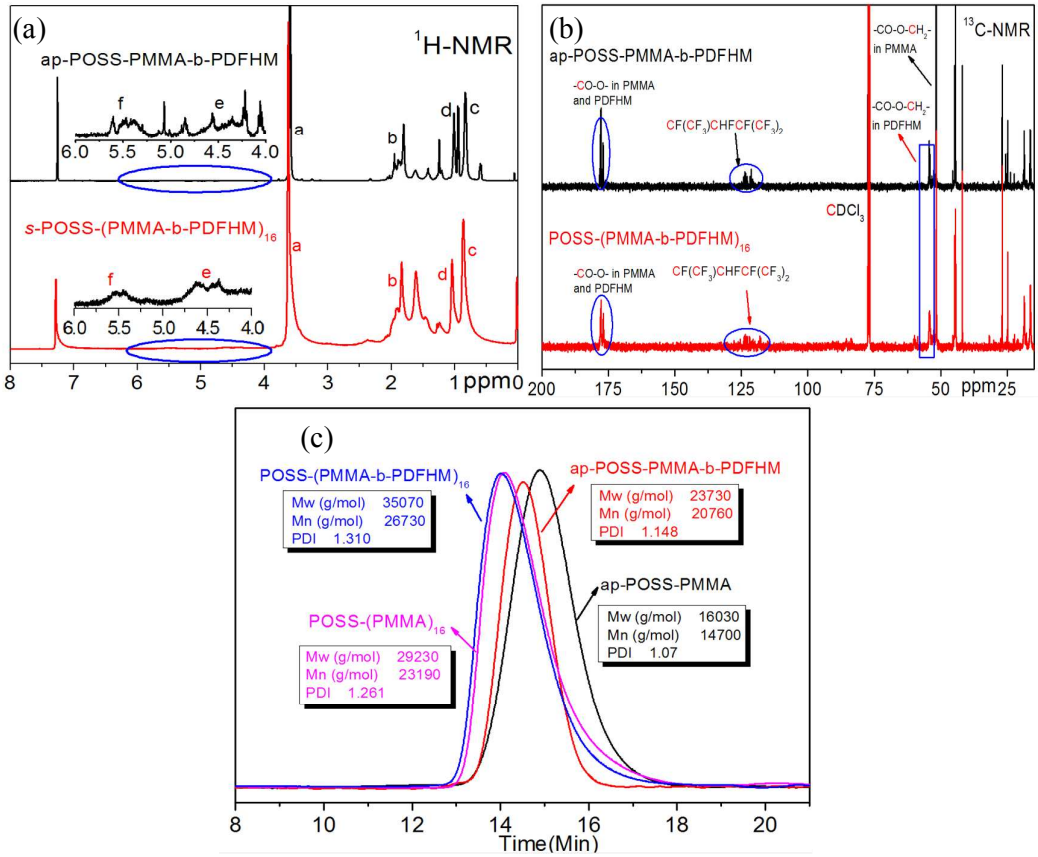

Fig. 1. ^{1}H-NMR (a), ^{13}C-NMR (b) spectra and SEC curves (c) of POSS-(PMMA-b-PDFHM)$_{16}$ and ap-POSS-PMMA-b-PDFHM

On the other hand, the molecular weights of 29230 g·mol^{-1} for POSS-(PMMA)$_{16}$ (PDI=1.261) and 35070 g·mol^{-1} for *s*-POSS-(PMMA-b-PDFHM)$_{16}$ (PDI=1.310) from SEC results (Fig. 1c) indicate that POSS-(Br)$_{16}$ initiator shows the similar wide distribution in the molecular weight to

POSS-$(Cl)_8$ initiator in ATRP approach (PDI=1.61-1.66 [26] and PDI=1.3-1.4).[36] These molecular weight distributions are really higher than EiBB for E-PMMA-b-PDFHM (Mn=34130 $g \cdot mol^{-1}$, PDI=1.115), ap-POSS for ap-POSS-PMMA (Mn=16030 $g \cdot mol^{-1}$, PDI=1.07) and ap-POSS-PMMA-b-PDFHM (Mn=23730 $g \cdot mol^{-1}$, PDI=1.148) (Fig. 1c). Furthermore, the calculated molecular weight of ap-POSS-PMMA-PDFHM from Fig. 1a of 21286 $g \cdot mol^{-1}$ (Supporting Information S1) is nearly matched well with the SEC results (Mn=23730 $g \cdot mol^{-1}$).

3.2 The self-assembled micelles in solution

The self-assembled micelles of two topological diblock copolymers in THF solution are observed in Fig. 2. Both *s*-POSS-$(PMMA\text{-}b\text{-}PDFHM)_{16}$ (Fig. 2a) and ap-POSS-PMMA-b-PDFHM (Fig. 2c) are able to self-assemble into 200 nm core/shell micelles with 70-80 nm thickness of shell. Through comparing with 110 nm POSS core/PMMA shell micelles for *s*-POSS-$(PMMA)_{16}$ (Fig. 2b), the core/shell micelles for *s*-POSS-$(PMMA\text{-}b\text{-}PDFHM)_{16}$ are composed of POSS/PDFHM inner core and PMMA shell (Fig. 2a), because both PDFHM and POSS have less solubility than PMMA and therefore are able to shrink into the inner core. But for ap-POSS-PMMA-b-PDFHM (Fig. 2c), the inner core looks like plum blossom (non-circularity) due to the obvious phase separation of ap-POSS and PMMA, and the size of plum blossom core is smaller than the core in the micelles formed by *s*-POSS-$(PMMA\text{-}b\text{-}PDFHM)_{16}$. Furthermore, compared with 80-100 nm spade-like micelles composed of PMMA spade top (the light part) and ap-POSS spade tail (15-30 nm, the dark part) for ap-POSS-PMMA (Fig. 2d), this plum blossom morphology is proved as PMMA shell and POSS/PDFHM core (Fig. 2c).

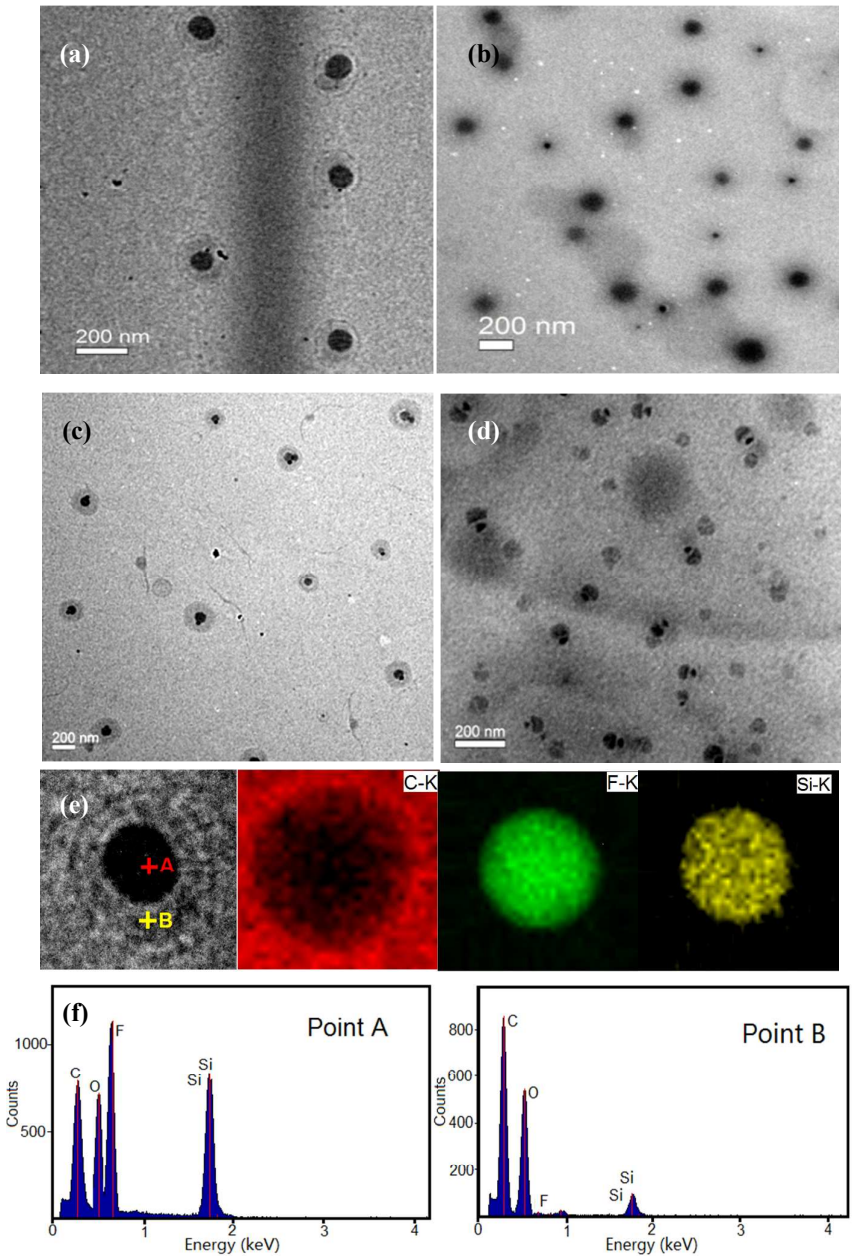

Fig. 2. TEM morphology of *s*-POSS-(PMMA-b-PDFHM)$_{16}$ (a), *s*-POSS-(PMMA)$_{16}$ (b), ap-POSS-PMMA-b-PDFHM (c) and ap-POSS-PMMA (d), TEM-EDX mapping of *s*-POSS-(PMMA-b-PDFHM)$_{16}$ (e and f) in THF solution

In order to confirm these specific morphology of micelles, both elemental mapping (Fig. 2e) and element distribution (Fig. 2f) of the core/shell structure by *s*-POSS-(PMMA-b-PDFHM)$_{16}$ are analyzed. The elemental mapping in Fig. 2e clearly reveals the spherical distribution of F and Si

elements in the inner core, and circular distribution of C element in the shell. The detailed element distribution of C, F and Si in inner black core (Fig. 2f, point A) indicates the dominant content of F and Si element which come from the PFMA segments and POSS cages, but the detailed element distribution of C, F and Si in the micelle shell (Fig. 2f, point B) present lower content of F and Si element but higher C and O contents from PMMA indicates that the shell is composed mainly of PMMA segments. Therefore, the EDX mapping and element distribution demonstrate that the inner core is made of PFMA/POSS due to their poor solubility and the shell is composed of PMMA segments. These different micelles will control the migration of PDFHM segments and POSS cages onto the film surface during the film-formation.

3.3 Surface morphology and chemical composition of self-assembled films

The surface morphology and surface chemical composition of films casted from these self-assembled micelles are characterized by AFM and XPS in Fig. 3. Compared with 0.367 nm surface roughness (Ra) and 10 nm root mean square roughness (RMSR) for *s*-POSS-$(PMMA)_{16}$ film (Fig. 3a), the surface of *s*-POSS-$(PMMA\text{-}b\text{-}PDFHM)_{16}$ film (Fig. 3b) displays higher roughness (Ra=4.9 nm, RMSR=50 nm) and uniform convexes by the strong driving force of PDFHM segments migrating onto the film surface compared with PMMA segments,[37,38] and therefore improve remarkably the surface roughness, which has been confirmed by the previous study.[7,8] While, for the surface of ap-POSS-PMMA-b-PDFHM film (Fig. 3c), much rough surface is observed (Ra=18.5 nm and RMSR=100 nm. Thus, it is possible to suggest that PDFHM segment in ap-POSS-PMMA-b-PDFHM is much easier migrating onto the film surface than that in *s*-POSS-$(PMMA\text{-}b\text{-}PDFHM)_{16}$, because the strong interaction between PMMA-b-PDFHM chains in

s-POSS-(PMMA-b-PDFHM)$_{16}$ around the POSS cage might limit the movement of its migration during the film formation.

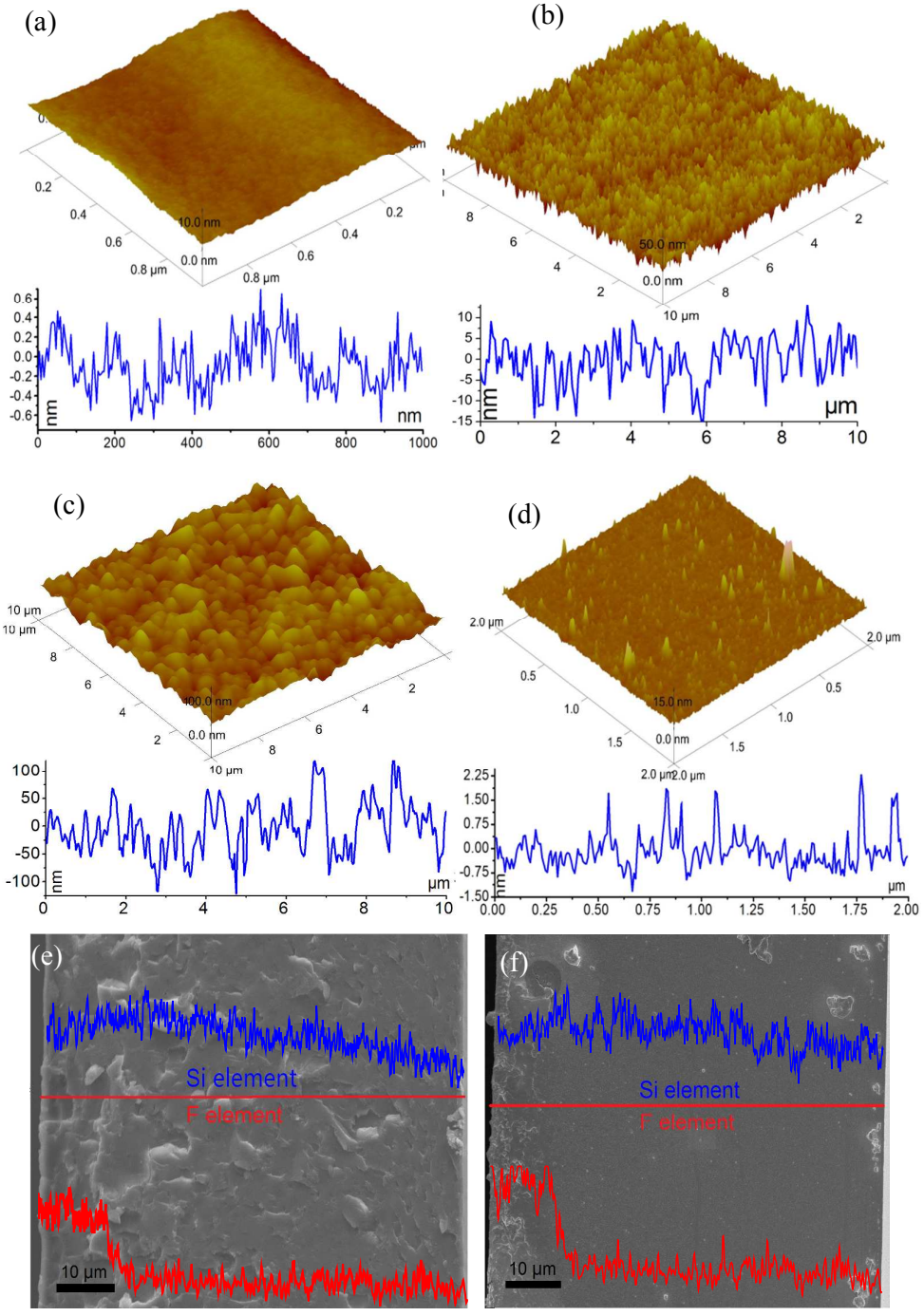

Fig. 3. AFM images of the film surface for *s*-POSS-(PMMA)$_{16}$ (a), *s*-POSS-(PMMA-b-PDFHM)$_{16}$ (b), ap-POSS-PMMA-b-PDFHM (c), for E-PMMA-b-PDFHM (d), and SEM-EDX plots for the

distribution profile of Si and F element on the surface of *s*-POSS-(PMMA-b-PDFHM)$_{16}$ film (e) and ap-POSS-PMMA-b-PDFHM film (f)

Fortunately, this migration is also proved by the chemical composition on the film surface in Table 2. Firstly, the fluorine content on the film surface is much higher than the powder for both *s*-POSS-(PMMA-b-PDFHM)$_{16}$ (41.39% for film and 15.05% for powder) and ap-POSS-PMMA-b-PDFHM (61.56% for film and 9.81% for powder), which distinctly indicates the migration of PDFHM segments onto the film surface. Secondly, compared with their powder, much higher increasing percentage of fluorine content on the surface of ap-POSS-PMMA-b-PDFHM film (527%) than that on *s*-POSS-(PMMA-b-PDFHM)$_{16}$ film (175%) in Table 2 further proves that PDFHM segment in ap-POSS-PMMA-b-PDFHM is much easier migrating onto the film surface than that in *s*-POSS-(PMMA-b-PDFHM)$_{16}$. Furthermore, the distribution profile of SEM-EDX on the surface of *s*-POSS-(PMMA-b-PDFHM)$_{16}$ film (Fig. 3e) and ap-POSS-PMMA-b-PDFHM film (Fig. 3f) also prove the higher content distribution of fluorine on the top surface of films (bottom red lines of Fig. 3e and f).

In order to understand the function of POSS cages during the film formation, E-PMMA-b-PDFHM film is analyzed by AFM and XPS. Much more smooth surface for E-PMMA-b-PDFHM film (3.70 nm Ra and 15 nm RMSR in Fig. 3d) than ap-POSS-PMMA-PDFHM film (Ra=18.5 nm) indicates that POSS cages could improve the migration of PDFHM segments onto the film surface, and therefore increase the surface roughness of films,[24] which is also proved by the fact that 105% increasing percentage of fluorine content on

E-PMMA-PDFHM film (from 18.49% for powder to 37.90% for film) is much lower than that in *s*-POSS-(PMMA-b-PDFHM)$_{16}$ and ap-POSS-PMMA-PDFHM films. Actually, Table 2 shows that the silicon content on the film surface is lower than its powder because of the enrichment of fluorine on the top surface, but the silicon element in both *s*-POSS-(PMMA-b-PDFHM)$_{16}$ and ap-POSS-PMMA-PDFHM films is actually enriched in the upper surface but not on the topsurface as determined in the cross section of film by SEM-EDX (upper blue lines of Fig. 3e and f), suggesting that POSS cages could also migrate onto the film surface, which is also proved by our previous study of ap-POSS and P(MA-POSS).[34] On the other hand, the decreasing of silicon content in ap-POSS-PMMA-PDFHM film surface (90%) is much higher than that on *s*-POSS-(PMMA-b-PDFHM)$_{16}$ film (15%), because the strong migration of PDFHM segment in *s*-POSS-(PMMA-b-PDFHM)$_{16}$ film limits the migration of POSS cages. Of course, the limitation of migration of PDFHM segments to POSS cages in ap-POSS-PMMA-PDFHM is much serious than that in *s*-POSS-(PMMA-b-PDFHM)$_{16}$. Therefore, the self-assembled films show the typical structures as fluorine-rich topsurface and POSS-gather subsurface.

Therefore, there must be a competition migration between POSS and PDFHM onto the film surface during the film formation by self-assembled micelles. Due to the migration of PDFHM segments onto the top surface, both *s*-POSS-(PMMA-b-PDFHM)$_{16}$ and ap-POSS-PMMA-b-PDFHM films obtain the fluorine-rich topsurface (Table 2), which is similar to other literatures,[4-6] but silicon element in *s*-POSS-(PMMA-b-PDFHM)$_{16}$ film (Fig. 3e, blue line) is also enriched in the subsurface, suggesting that POSS cages could also migrate onto the film surface, but this migrating is much difficulty than PDFHM segment, so as to gather in the subsurface (Scheme 2). In this case, PMMA

segments are of course distributed mainly in the bottom layer of film. Therefore, it is possible to conjectured that the self-assembled *s*-POSS-(PMMA-b-PDFHM)$_{16}$ and ap-POSS-PMMA-b-PDFHM films are distributed as fluorine-rich topsurface/POSS-gather subsurface structure of films (Scheme 2), and the arranged fluorine groups on the topsurface in ap-POSS-PMMA-b-PDFHM film are much denser than on *s*-POSS-(PMMA-b-PDFHM)$_{16}$ film (Scheme 2).

Table 2 Surface roughness and chemical composition, viscoelasticity ($\Delta D/\Delta f$) and water absorption (Δf) of self-assembled films

Copolymer samples	Solid state	Surface roughness/nm	Chemical composition /wt%	ΔD/Δf $\times10^{-6}$ Hz^{-1}	Δf /Hz
		Ra/RMSR	C/O/F/Si		
s-POSS-(PMMA)$_{16}$	Film	0.367/10	-	-0.077	-1300
s-POSS-(PMMA-b-PDFHM)$_{16}$	Powder	-	47.80/36.18/15.05*/0.97	-	-
	Film	4.9/50	34.42/23.37/41.39*/0.82	-0.27	-290
ap-POSS-PMMA-b-PDFHM	Powder	-	51.37/37.85/9.81*/0.97	-	-
	Film	18.5/100	23.94/14.41/61.56*/0.09	-0.15	-315
E-PMMA-b-PDFHM	Powder	-	58.04/23.47/18.49/0	-	-
	Film	3.70/15	43.46/18.64/37.90/0	-0.29	-650

* The increasing percentage of fluorine content on ap-POSS-PMMA-b-PDFHM film (527%) is much higher than that on *s*-POSS-(PMMA-b-PDFHM)$_{16}$ film (175%) compared with their powders.

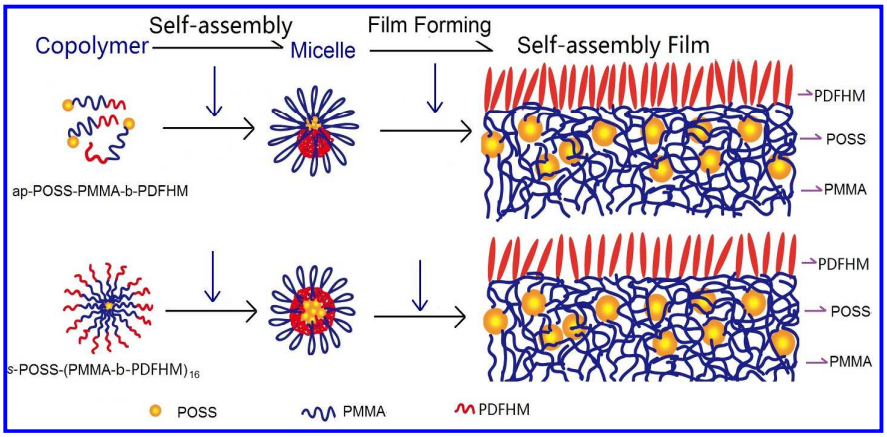

Scheme 2. The formation of *s*-POSS-(PMMA-b-PDFHM)$_{16}$ and ap-POSS-PMMA-b-PDFHM films

3.4 Surface water adsorption and viscoelasticity of films

The fluorine-rich and rough surface formed by the migration of PDFHM segments contributes much to the surface water adsorption and viscoelasticity of films, which is proved by the QCM-D measurement in Fig. 4. The Δf in the adsorption curves is used to indicate the adsorbed amounts of probe liquids, and the $\Delta D/\Delta f$ at the end of adsorption is used to indicate the viscoelasticity of the adsorbed layer (the higher $\Delta D/\Delta f$ value indicates the softer adsorbed layer). For *s*-POSS-(PMMA-b-PDFHM)$_{16}$ film (Fig. 4a), the ΔD increases with the decrease of Δf at 0-40 minute suggests that the adsorbed water is loosely arranged on the film surface due to the fluorine-rich surface resisting the adsorbed water penetrating deeply. While, the sudden increasing and then decreasing of ΔD with the increasing of Δf at 40-50 minutes suggest that the PDFHM segments have regulated into orientated in the adsorbed layer (Fig. 4e), which plays the crucial function in further water resistance. Therefore, *s*-POSS-(PMMA-b-PDFHM)$_{16}$ film obtains a much harder viscoelasticity adsorbed layer as $\Delta D/\Delta f$=-0.27×10^{-6} Hz^{-1} and much lower water adsorption (Δf=-290 Hz) at the end adsorption equilibrium at 55 minutes, compared with a soft adsorbed layer of $\Delta D/\Delta f$=-0.077 ×10^{-6} Hz^{-1} and higher water adsorption of Δf=-1300 Hz for *s*-POSS-(PMMA)$_{16}$ film (Fig. 4b). But for ap-POSS-PMMA-b-PDFHM film in Fig. 4c, the increasing of ΔD with the decreasing of Δf at 10-25 minutes suggests that the film gives the obvious resistance to water adsorption and reaches the equilibrium at a short time (25 minutes) than *s*-POSS-(PMMA-b-PDFHM)$_{16}$ film due to its much fluorine-richer surface (Table 2), which is corresponding to the result that *s*-POSS-(PMMA-b-PDFHM)$_{16}$ film gains the higher water contact angles (122°) compared with ap-POSS-PMMA-b-PDFHM film (112°) (Table 3). In this case, ap-POSS-PMMA-b-PDFHM film gains a soft adsorbed layer (i.e. lower viscoelasticity,

$\Delta D/\Delta f$=-0.15×10^{-6} Hz^{-1}) and a little higher water adsorption (Δf=-315 Hz) at the end adsorption than *s*-POSS-(PMMA-b-PDFHM)$_{16}$ film ($\Delta D/\Delta f$=-0.27×10^{-6} Hz^{-1}, Δf=-290 Hz). While, due to the contribution of POSS cages, ap-POSS-PMMA-b-PDFHM film gains lower water adsorption and lower viscoelasticity than E-PMMA-b-PDFHM film (Δf=-650Hz, $\Delta D/\Delta f$=-0.29×10^{-6} Hz^{-1}, Fig. 4d).

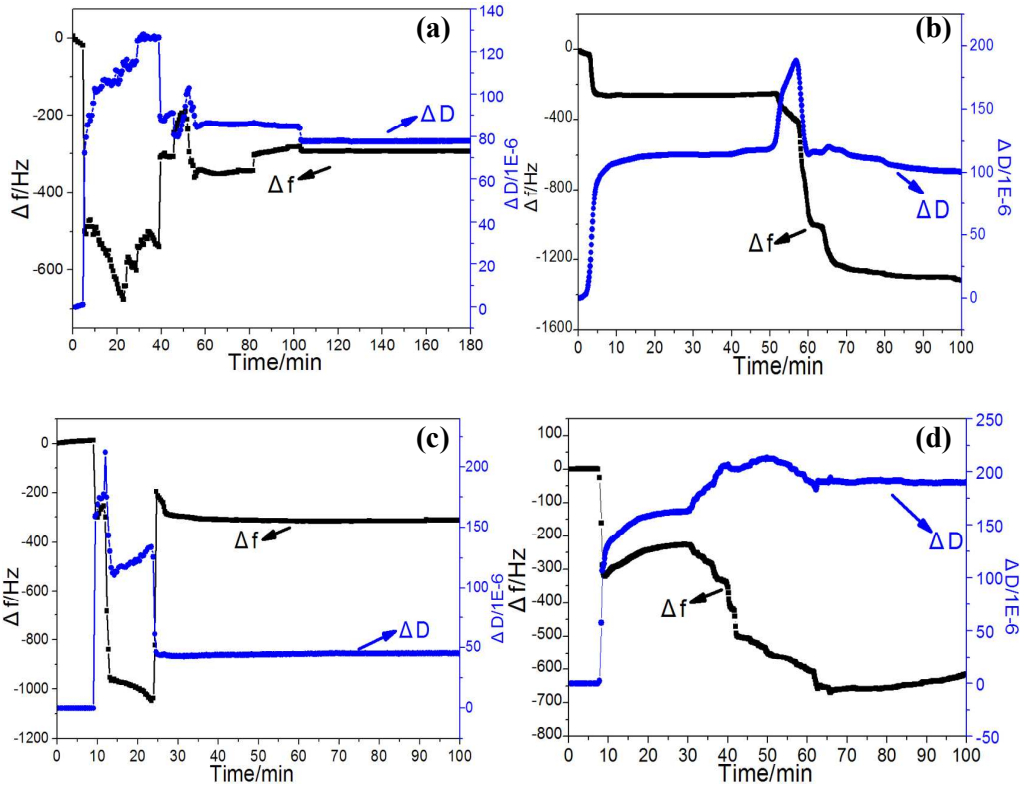

Fig. 4. The QCM-D data of Δf and ΔD of *s*-POSS-(PMMA-b-PDFHM)$_{16}$ (a), *s*-POSS-(PMMA)$_{16}$ (b), ap-POSS-PMMA-b-PDFHM (c) and E-PMMA-b-PDFHM (d) films, and the water adsorption mechanism of films (e)

3.5 Hydrophobic application to substrates

The hydrophobic application to three different substrates of the glass sheets, stone and cotton fabric are used to evaluate the regulating and controlling the surface properties, and are investigated by SEM and water contact angle of advancing contact angles (θ_A), receding contact angles (θ_R) and static contact angles (θ_s) in Table 3. For the treated surface on the glass sheet, *s*-POSS-(PMMA-b-PDFHM)$_{16}$ film gains higher hydrophobicity (θ_A=124.7°, θ_R=119.6°, θ_s=122°) than ap-POSS-PMMA-b-PDFHM film (θ_A=114.8, θ_R=109.5°, θ_s=112°), although both of them have the similar contact angle hysteresis ($\Delta\theta_{A-R}$=5.1-5.3°). But the higher fluorine content on the surface of ap-POSS-PMMA-b-PDFHM film endows its higher oleophobicity (methylene iodide contact angles θ_{mi-s}=74.8°) than *s*-POSS-(PMMA-b-PDFHM)$_{16}$ film (θ_{mi-s}=66.5°). Therefore, ap-POSS-PMMA-b-PDFHM film obtains lower hydrophobicity (θ_A=124.7°, θ_R=119.6°, θ_s=122°) but higher oleophobicity than *s*-POSS-(PMMA-b-PDFHM)$_{16}$ film.

Table 3. The advancing, receding and static water contact angles of protective surface

Copolymer sample	Substrates*	Water contact angles/º				Methylene iodide contact angles/º
		θ_A	θ_R	$\Delta\theta_{A-R}$	θ_S	θ_{mi-S}
s-POSS-(PMMA-b-PDFHM)$_{16}$	Glass sheets	124.7	119.6	5.1	122.0	66.5
	Cotton fabrics	155.8	152.4	3.4	153.2	112.8
	Stones	141.5	134.9	6.6	136.8	91.5
ap-POSS-PMMA-b-PDFHM	Glass sheets	114.8	109.5	5.3	112.0	74.8
	Cotton fabrics	160.5	157.6	2.9	158.1	129.2
	Stones	150.2	143.8	6.4	145.9	103.5

*: As for the water contact angles of untreated substrates, θ_s=54º for the untreated glass sheets, θ_s=0º for the untreated cotton fabrics and untreated stones.

On the other hand, the treated fabrics by both copolymers achieve superhydrophobic surface as the largest θ_A (155.8° and 160.5°) and θ_R (152.4° and 157.6°), and the smallest $\Delta\theta_{A-R}$ (2.9-3.4°).

While the treated stones by both copolymers own high hydrophobic property as θ_A (141.5° and 150.2°) and θ_R (134.9° and 143.8°) with the largest $\Delta\theta$ (6.4-6.6°). All the treated fabric and stone samples by ap-POSS-PMMA-b-PDFHM have higher water contact angles and methylene iodide contact angles than *s*-POSS-(PMMA-b-PDFHM)$_{16}$. Therefore, these super or high hydrophobic surfaces are related to the typical rough surface of substrates. As it is known, the super or high hydrophobic surfaces are related to the micro/nano-scale rough surface of substrates. Because the glass sheets have the smoothest surface among three substrates, therefore, the hydrophobic effect are only controlled by the coated copolymer which have the smaller roughness in nano-scale as discussed in Fig. 3 and Table 2. However, the stone and cotton fabric could provide the micro-scale rough surface. And the copolymer could provide nano-scale rough surface. Therefore, the micro/nano-scale rough surface could provide the coated surface water much higher contact angles than the coated glass sheets. Therefore, the treated stone samples (Fig. 5-a and b) and fabric samples (Fig. 5-c and d) present obviously convex and concaves, much rougher than the uncoated stones (Fig. S2-a and b) and highly-smoothed glass substrate. On the other hand, the treated stone by star-shaped copolymer is much more uniform than the treated one by linear-shaped copolymer, which makes ap-POSS-PMMA-b-PDFHM have higher water contact angles than *s*-POSS-(PMMA-b-PDFHM)$_{16}$. Actually, the superhydrophobic surface for the treated fabrics than the treated stones is attributed to the treated cotton fabric samples with a relative rough layer and low bulges on the micro-fiber surfaces (Fig. 5-c and d) compared with the smoothing surface of the uncoated fabrics (Fig. S2). In addition, both linear- and star-shaped diblock copolymers also exhibit superhydrophobicity to fabric

and high-hydrophobicity to stones in resistance to other liquids as coffee, milk, coke and green tea (Fig. 6 and Fig. S3).

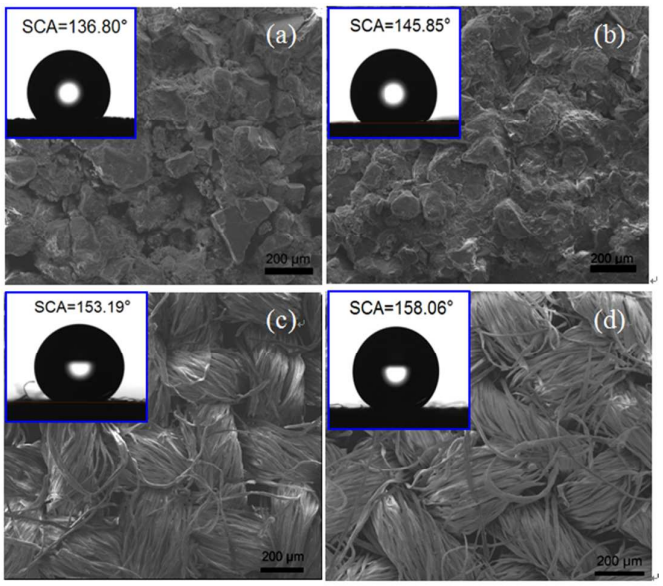

Fig. 5. SEM images of treated stones and cotton fiber by *s*-POSS-(PMMA-b-PDFHM)$_{16}$ (a, c) and ap-POSS-PMMA-b-PDFHM (b, d)

Fig. 6. The hydrophobicity of treated stones and cotton fabric to water, coffee, milk, coke and tea

4. Conclusion

POSS-tethered fluorinated diblock copolymers of linear-shaped ap-POSS-PMMA-b-PDFHM and star-shaped *s*-POSS-(PMMA-b-PDFHM)$_{16}$ are synthesized. Their self-assembled films are proved as

fluorine-rich topsurface and POSS-gathered subsurface casted from 200 nm POSS/PDFHM core and PMMA shell micelles in THF solution. This typical surface is built by the competitive migrating between PDFHM segments and POSS cages, but POSS cages could improve the migration of PDFHM segments onto the film surface to increase the surface roughness of films. Since PDFHM segment in ap-POSS-PMMA-b-PDFHM is much easier migrating onto the film surface than that in *s*-POSS-(PMMA-b-PDFHM)$_{16}$, the surface of ap-POSS-PMMA-b-PDFHM film is much more rough (Ra=18.5nm) and fluorine-rich (61.56%) than *s*-POSS-(PMMA-b-PDFHM)$_{16}$ film ((Ra=18.5nm and F%=41.39%). Therefore, ap-POSS-PMMA-b-PDFHM film gains higher water adsorption and viscoelasticity than *s*-POSS-(PMMA-b-PDFHM)$_{16}$ film. The protective treated fabrics achieve superhydrophobic surface (>153°), the treated stones own high hydrophobicity (>136°) and the treated glasses get enough hydrophobicity (>112°). All the treated fabric and stone samples by ap-POSS-PMMA-b-PDFHM have higher water contact angles than *s*-POSS-(PMMA-b-PDFHM)$_{16}$. Therefore, the linear-shaped ap-POSS-PMMA-b-PDFHM shows better hydrophobicity than the star-shaped *s*-POSS-(PMMA-b-PDFHM)$_{16}$ in resistance to water, coffee, milk, coke and green tea.

Acknowledgements

This work has been financially supported by the National Natural Science Foundation of China (NSFC Grants 51373133, 51073126), by the National Basic Research Program of China (973 Program, No.2012CB720904), by the and by the International Cooperation Project of Shaanxi Province (No.2014KW11) and the State Administration of Cultural Heritage (20110128). The authors also wish to express their gratitude for the MOE Key Laboratory for Non-equilibrium

Condensed Matter and Quantum Engineering of Xi'an Jiaotong University.

References

1 I. W. Hamley, *Prog. Polym. Sci.,* 2009, **34**, 1161-1210.

2 M. Han, M. S. Rahman, J. S. Lee, D. Khim, D. Y. Kim and J. W. Park, *Chem. Mater.,* 2011, **23**, 3517-3524.

3 D. Xiong, G. Liu, J. Zhang and L. Hong, *Chem. Mater.,* 2011, **23**, 4357-4366.

4 Y. Koda, T. Terashima, A. Nomura, M. Ouchi and M. Sawamoto, *Macromolecules,* 2011, **44**, 4574-4578.

5 C. Tang, W. Liu, S. Ma, Z. Wang and C. Hu, *Prog. Org. Coat.,* 2010, **69**, 359-365.

6 K. Y. Mya, E. M. J. Lin, C. S. Gudipati, H. B. A. S. Gose and C. He, *J. Phys. Chem. B,* 2010, **114**, 9128-9134.

7 X. Dong, L. He, N. Wang, J. Y. Liang, M. J. Niu and X. Zhao, *J. Mater. Chem.,* 2012, **22**, 23078-23090.

8 J. Liang, L. He, X. Zhao, X. Dong, H. Luo and W. Li, *J. Mater. Chem.,* 2011, **21**, 6934-6943.

9 D. B. Cordes, P. D. Lickiss and F. Rataboul, *Chem. Rev.,* 2010, **110**, 2081-2173.

10 S. W. Kuo and F. C. Chang, *Prog. Polym. Sci.,* 2011, **36**, 1649-1696.

11 A. J. Guenthner, K. R. Lamison, L. M. Lubin, T. S. Haddad and J. M. Mabry, *Ind. Eng. Chem. Res.,* 2012, **51**, 12282-12293.

12 O. Monticelli, A. Fina, E. S. Cozza, M. Pratoc and V. Bruzzo, *J. Mater. Chem.,* 2011, **21**, 18049-18054.

13 P. Chen, X. Huang, Q. Zhang, K. Xi and X. Jia, *Polymer,* 2013, **54**, 1091-1097.

14 O. Monticelli, A. Fina, A. Ullah and P. Waghmare, *Macromolecules,* 2009, **42**, 6614-6623.

15 A. Fina, D. Tabuani, T. Peijs and G. Camino, *Polymer,* 2009, **50**, 218-226.

16 S. M. Ramirez, Y. J. Diaz, C. M. Sahagun, M. W. Duff, O. B. Lawal, S. T. Iaconoc and J. M. Mabry, *Polym. Chem.,* 2013, **4**, 2230-2234.

17 Y. C. Lin and S. W. Kuo, *Polym. Chem.,* 2012, **3**, 882-891.

18 K. Wei, L. Li, S. Zheng, G. Wang and Q. Liang, *Soft Matter,* 2014, **10**, 383-394.

19 J. N. Martins, T. S. Bassani and R. V. B. Oliveira, *Mat. Sci. Eng. C.,* 2012, **32**, 146.

20 C. H. Liao, F. M. Chien, C. M. Chen, L. C. Liu, M. H.Chung and F. C. Chang, *Mater. Chem. Phys.,* 2011, **131**, 343-347.

21 F. Alves, P. Scholder and I. Nischang, *ACS Appl. Mater. Interfaces,* 2013, **5**, 2517-2526.

22 J. Wu, Q. Ge and P. T. Mather, *Macromolecules,* 2010, **43**, 7637-7649.

23 B. H. Tan, H. Hussain, T. T. Lin, Y. C. Chua, Y. W. Leong, W. W. Tjiu, P. K. Wong and C. B. He, *Langmuir,* 2011, **27**, 10538-10547.

24 L. Ma, H. Geng, J. Song, J. Li, G. Chen and Q. Li, *J. Phys. Chem. B,* 2011, **115**, 10586-10591.

25 W. Zhang and A. H. E. Müller, *Macromolecules,* 2010, **43**, 3148-3152.

26 W. Wang, M. Fei, X. Jie, P. Wang, H. Cao and J. Yu, *Polym. Bull.,* 2010, **65**, 863-872.

27 A. G. Kannan, N. R. Choudhury and N. Dutta, *ACS Appl. Mater. Interfaces,* 2009, **1**, 336-347.

28 H. Fujiwara, T. Narita and H. Hamana, *J. Fluorine Chem.,* 2004, **125**, 1279-1285.

29 Y. Gan, X. Jiang and J. Yin, *Macromolecules,* 2012, **45**, 7520-7526.

30 M. E. Wright, B. J. Petteys, A. J. Guenthner, S. Fallis, G. R. Yandek, S. J. Tomczak, T. K. Minton and A. Brunsvold, *Macromolecules,* 2006, **39**, 4710-4718.

31 B. Sharma, R. Verma, C. Baur, J. Bykova, J. M. Mabry, D. W. Smith Jr., J. Mater. Chem. C 2013, **1**, 7222-7227.

32 S. T. Iacono, S. M. Budy, D. W. Smith and J. M. Mabry Jr., *J. Mater. Chem.,* 2010, **20**, 2979-2984.

33 V. A. Ganesh, A. S. Nair, H. K. Raut, T. T. Y. Tan, C. He, S. Ramakrishna and J. Xu, *J. Mater. Chem.,* 2012, **22**, 18479-18485.

34 S. Yang, A. Pan and L. He, *J. Colloid Interface Sci.,* 2014, **425**, 5-11.

35 A. Pan and L. He, *J. Colloid Interface Sci.,* 2014, **414**, 1-8.

36 W. Yuan, T. Shen, X. Liu and J. Ren, *Mater. Lett.,* 2013, **111**, 9-12.

37 M. Niu, L. He, J. Liang, A. Pan and X. Zhao, *Prog. Org. Coat.,* 2014, **77**, 1603-1612.

38 C. Zhang, S. Guang, X. Zhu, H. Xu, X. Liu and M. Jiang, *J. Phys. Chem. C,* 2010, **114**, 22455-22461.